Int. J. Electrochem. Sci., 9 **(2014)** 5012 - 5024

International Journal of
ELECTROCHEMICAL
SCIENCE
www.electrochemsci.org

Effect of Anodization time on Morphology and Electrochemical Impedance of Andic Oxide Films on Titanium Alloy in Tartrate Solution

Liang Wu, Jianhua Liu[*]*, Mei Yu, Songmei Li, Hongxing Liang, Mengqi Zhu*

School of Materials Science and Engineering, Beihang University, Beijing 100191, China
[*]E-mail: liujh@buaa.edu.cn

Received: 20 May 2014 / *Accepted:* 7 June 2014 / *Published:* 16 June 2014

The present study investigated the effect of anodization time on the anodic oxide films formed on titanium alloy Ti-6Al-2Zr-1Mo-1V. The morphology, surface roughness, crystal structure, and electrochemical impedance of the anodic oxide films were studied by using scanning electron microscopy (SEM), atomic force microscopy (AFM), Raman spectroscopy, electrochemical impedance spectroscopy (EIS), respectively. At the beginning of the anodization, a compact inner layer was form on the substrate. With elongated anodization time, the inner layer ruptured locally and secondary oxide particles grew up. Finally, the secondary oxide particles aggregated in masses forming outer layer of anodic oxide films. The surface roughness of the oxide films increased firstly and then decreased. These results showed good correlation to the analysis of EIS. The results of Raman spectroscopy showed that the relative intensity of anatase and rutile had a tendency to increase with anodization time.

Keywords: Anodic oxide films, Titanium, Tartrate solution, Roughness, Electrochemical impedance

1. INTRODUCTION

Titanium alloy Ti-6Al-2Zr-1Mo-1V has been widely applied in aerospace industry for its superior room, elevated temperature mechanical properties [1]. However, additional surface treatment is usually required to improve the superficial mechanical properties (i.e., the wear resistance and superficial hardness), as well as the corrosion resistance of the titanium alloys [2, 3].

Anodization is a widely used method to form protective oxide films on titanium and its alloys [4-7]. The advantages of this technique include effortless manual work [8], strong adhesion between the oxide layer and the substrate [9], and facile control of the surface morphology [10-12]. The anodization of Ti and its alloys comprises primarily a simple process of applying an anodic current to

the substrate in the proper electrolyte solution. The parameters of anodization, such as electrolyte, temperature, anodic current density and anodization time, significantly affect the growth behavior and properties of the anodic oxide films[13-16].

In our previous work, thick, uniform and non-transparent anodic oxide films were fabricated on titanium alloy Ti-10V-2Fe-3Al and Ti-6Al-4V in an aqueous solution of sodium tartrate [17-20]. Influence of electrolyte concentration and anodizing current on morphology, microstructure and electrochemical corrosion properties of oxide film on titanium alloy Ti-10V-2Fe-3Al and Ti-6Al-4V were studied[17-20]. The growth of anodic oxide film was carried out in stages in our work. Therefore, the present work aims to evaluate the effect of anodization time on the morphology, surface roughness and electrochemical impedance of anodic oxide film on titanium alloy Ti-6Al-2Zr-1Mo-1V. Correlations among anodization time, surface roughness, crystal structure and electrochemical impedance of anodic oxide film were discussed.

2. EXPERIMENTAL

Titanium alloy plates with dimension of 50 × 25 × 3 mm were used as the substrates. The nominal chemical components of titanium alloy Ti-6Al-2Zr-1Mo-1V are shown in Table 1. Prior to anodization, samples were abraded with silicon carbide (SiC) paper of successive grades from 200 to 2000 grit and further mechanically polished to mirror finish with diamond paste of 1μm. All samples were then ultrasonically cleaned in ethanol solution, degreased in alkaline solution and rinsed in deionized water.

Table 1. Nominal chemical components of titanium alloy Ti-6Al-2Zr-1Mo-1V (wt%)

Al	Mo	V	Zr	Fe	Si	N	H	Ti
5.5~7.0	0.5~2.0	0.8~2.5	1.5~2.5	<.25	<0.15	<0.05	<0.015	Balance

Table 2. Parameters of anodizing processes

Parameters	Value(Unit)
Current density	10 A/dm^2
Duty ratio	20 %
Frequency	2Hz
Anodizing time	5,10,20,30min
Temperature	15±2 ℃
Agitation speed	200 rpm
Surface area ratio of cathode to anode	4:1

Anodization was carried out in an electrolytic cell with a magnetic stirring apparatus at 15±2℃. The prepared sample was used as anode, and a 1Cr18Ni9Ti stainless steel plate was used as cathode. The electrolyte was an aqueous solution of 0.2 M sodium tartrate ($C_4H_4O_6Na_2$), which was prepared using analytical grade chemicals and deionised water. A pulse galvanostatic power supply (WMY-IV,China) was used. The applied current pulse of the power supply was unidirectional and exhibited a square wave. The fabrication conditions are shown in Table 2.

The morphology and roughness of the anodized samples were examined by using SEM (S-4800, Hitachi, Japan) and AFM (Icon,Veeco, USA). The crystal structure characterization was carried out using Raman spectroscopy (Yvon Jobin Horiba-HR 800, He-Ne laser without filter, 650nm).

Electrochemical measurements were carried out using a potentiostat/galvanostat (Parstat 2273, Princeton Applied Research, USA) with a conventional three-electrode electrochemical cell wherein the samples functioned as the working electrode (WE), a platinum plate was the counter electrode (CE) and a saturated calomel electrode (SCE) was used as the reference electrode (RE). EIS measurement was conducted in the following way. After the anodic oxidation process, the sample was transferred into the traditional three-electrode cell. The electrolyte was 0.2 M sodium tartrate solution. The open circuit potential (OCP) measurements were done for 30min before impedance measurements were performed. The alternating current (AC) impedance spectra of samples were obtained at the open circuit potential, with an amplitude of 10 mV and a scan frequency range of 100 kHz to 10 mHz (10 points per decade). Bode plots were obtained by curve fitting using a commercial software package called Electrochemistry Power Suite^{TM}. The EIS spectra were simulated using the Zsimpwin simulation software.

3. RESULTS AND DISCUSSION

3.1 Effect of anodization time on the color of the anodic oxide films

Fig.1 shows the time transient of the anodizing voltage between the cathode and the anode during the anodization. The anodizing voltage increased in three stages. At the beginning of the anodization, the voltage increased abruptly up to about 107V within 5 min. The linear increase of anodizing forming voltage had been explained by the well-known high field-assisted ionic transport mechanism [21, 22]. Thereafter, the rate of increase was moderate until about 20min, whereupon its value reached about 123V. Finally, the anodization voltage was approximately maintained at a steady value. The voltage at 30min was about 124V. The result regarding the transition of voltage was similar to the result which was reported by S. Komiya et al. The growth of TiO_2 layer in 0.1 M $(NH_4)SO_4$ aqueous solution with different reaction times was progressed through three stages. At the first and second stages, the voltage increased abruptly, whereas the change of voltage was hardly observed at the third stage [13].

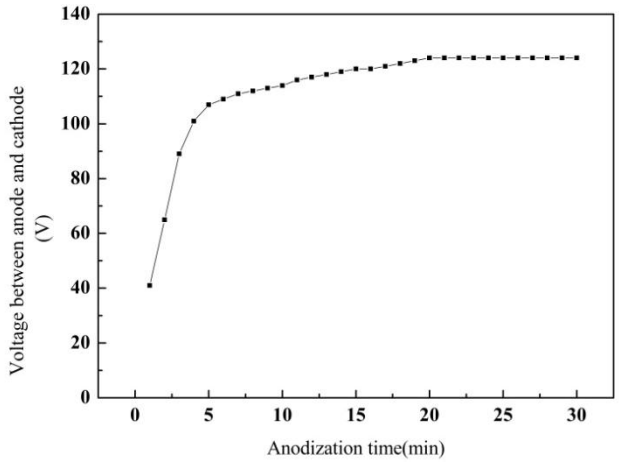

Figure 1. Anodic oxide films forming voltage-time plot for titanium alloy Ti-6Al-2Zr-1Mo-1V in 0.2 M sodium tartrate

Fig.2 shows the appearance of the anodizied substrates at different anodization time. The Ti substrate without anodization appears gray with metallic luster (Fig.2(a)). However, the substrate becomes blue by anodization at 5min (Fig.2(b)), indicating that a new oxide layer is formed on the surface. Furthermore, a lot of faint yellow spots appears on the surface of blue oxide layer at 10min (Fig.2(c)), indicating that another new oxide layer began to form. The entire substrate appears faint yellow at 20min (Fig.2(d)) and the blue oxide layer is covered. Finally, the colour of the film becomes yellow at 30min (Fig.2(e)). The coloring of the anodic oxide films can be explained by the multiple beam interference theory [23]. When the light source strikes the titanium oxide, there is an interference phenomenon between the reflected beam from the oxide surface and the beam which penetrates the surface oxide and titanium substrate. Therefore, interference colors are affected by the thickness of anodic oxide films.

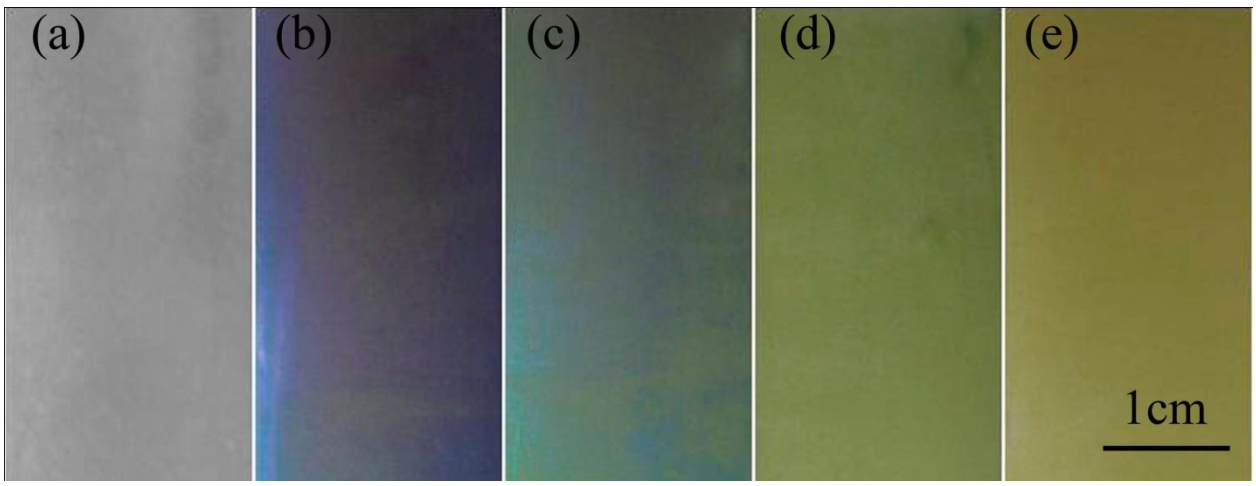

Figure 2. Optics images of the substrate(a) without anodization , and anodized in 0.2 M $C_4H_4O_6Na_2$ aqueous solution for(b) 5min,(c)10min,(d)20min,(e)30min.

3.2 Effect of anodization time on morphology of the anodic oxide films

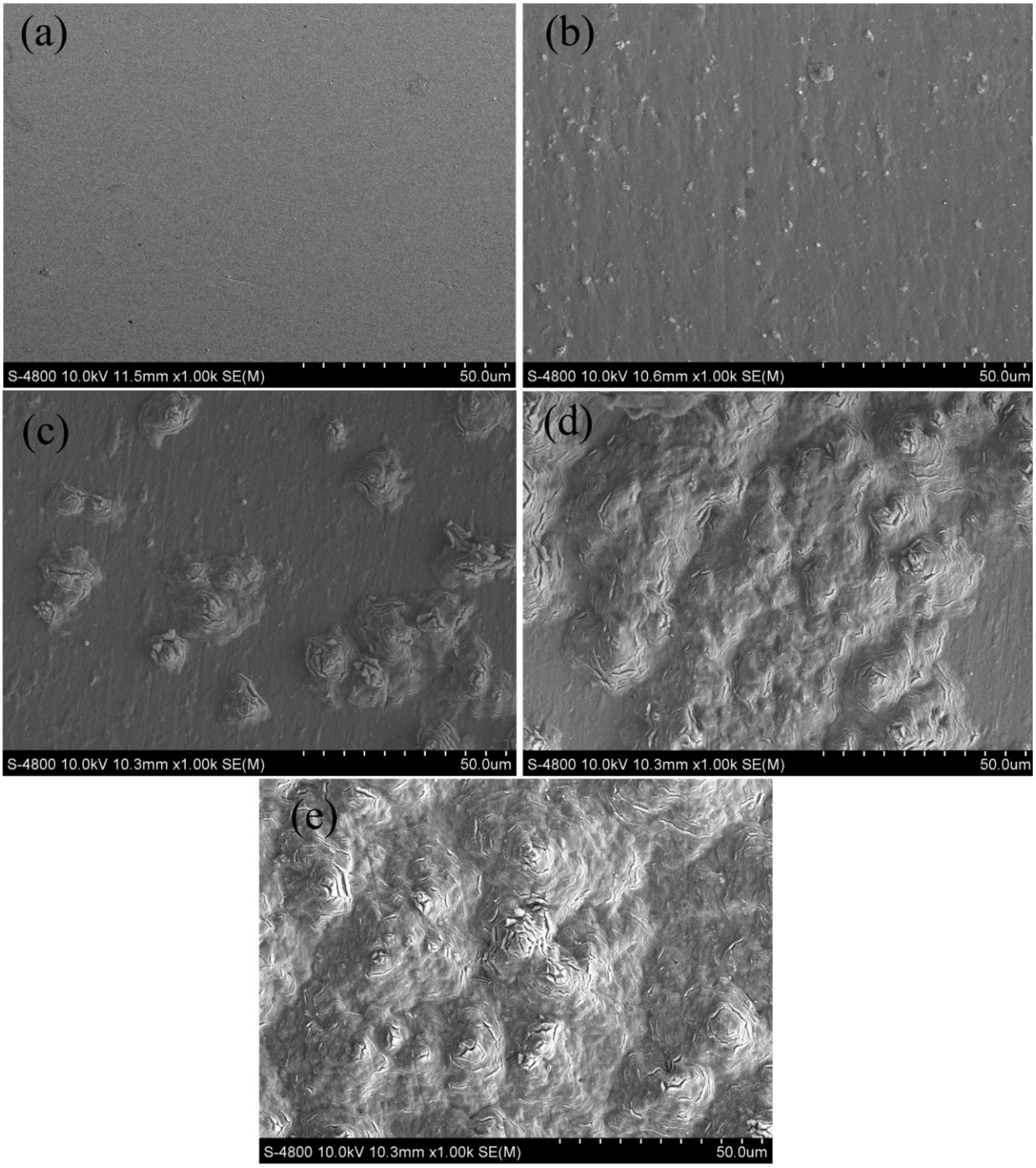

Figure 3. Surface morphology of the anodic oxide films on titanium alloy at different anodization time (a 0min, b 5min,c 10min,d 20min,e 30min)

Fig. 3 shows surface morphology of the films at different time of anodization processes. Before anodization, the surface of polished sample was smooth and homogenized (Fig. 3(a)). After 5min of anodization, corresponding to the first stage in Fig. 1, a compact inner layer was formed on the surface of Ti substrate and some small bumps were appeared in the inner layer. The small bumps were called

as secondary oxide particles because of that the difference between them and inner layer was very evident (Fig. 3(b)). At 10 min, Partial rupture of the compact inner layer and growth of secondary oxide particles were presented.

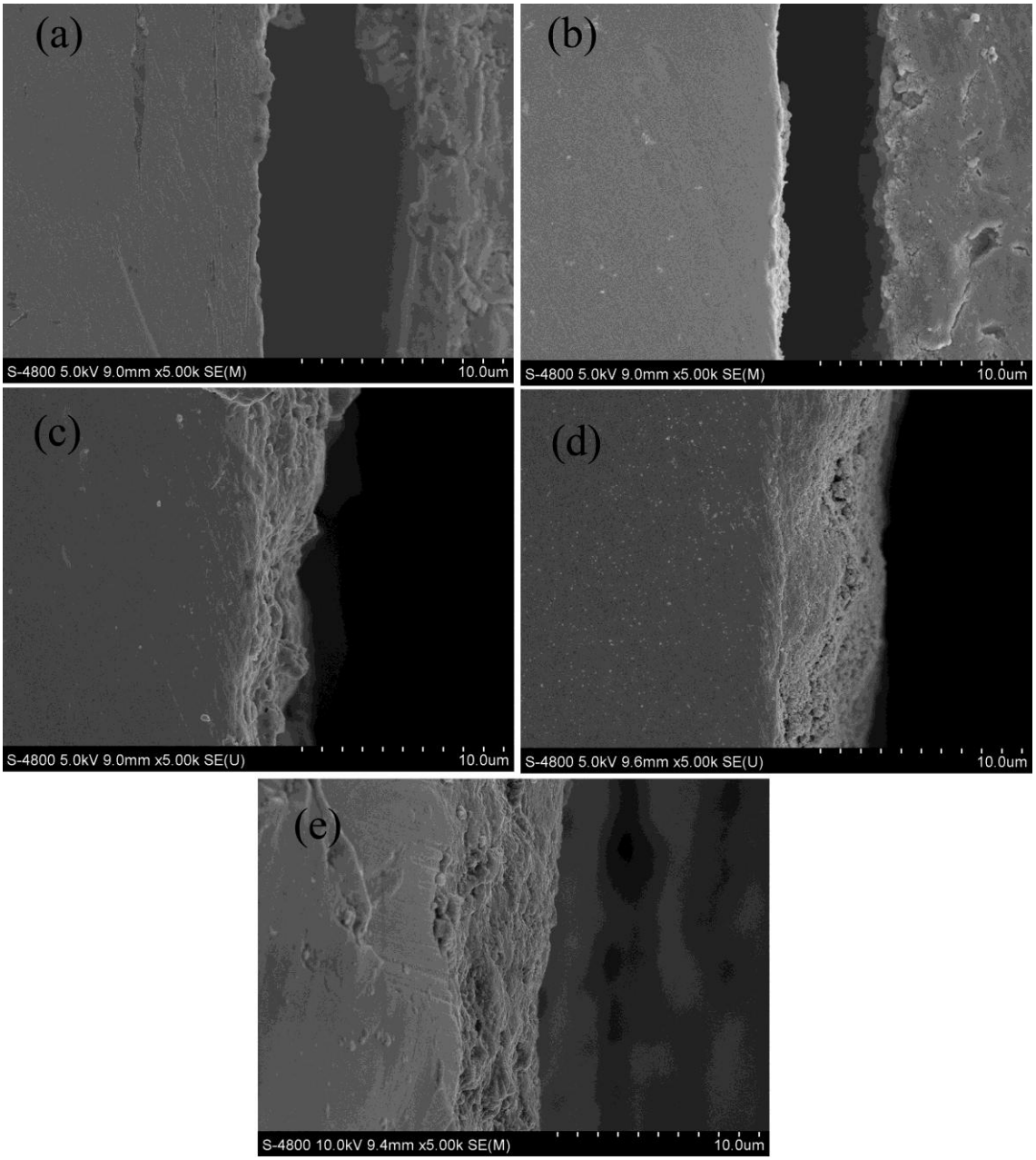

Figure 4. SEM images of cross-section of the anodic oxide films on titanium alloy at different anodization time (a 0min, b 5min,c 10min,d 20min,e 30min)

The shape of secondary oxide particles was like flower petal the amount of the secondary oxide particles evidently increased and some of them were connected together (Fig. 3(c)). At 20 min, almost the entire surface was covered with a layer of secondary oxide particles, except a few areas (Fig. 3(d)). At 30 min, all of secondary oxide particles merged together and the surface was entirely covered by

them (Fig. 3(e)). Habazaki et al. reported that vacancies due to the O2 bubbles existed in the inner region of the anodic TiO_2 layer fabricated using H_3PO_4[24].In addition, Zhu et al. considered that the generation of O_2 bubbles during anodization of aluminum resulted in the formation of the pourous surface morphology of the anodic alumina[25].Therefore, we thought that the structure of flower petal and the cracks in the films might be caused by the generation of O_2 bubbles during anodization. Furthermore, tartaric acid was a weak acid and the soluble reaction of films in tartaric acid was slower than that in strong acid. Therefore, petals and cracks were presented in the films instead of pores in our study.Fig.4 shows the cross-section images of the anodic oxide films fabricated at various anodization time. No oxide could be found at the interface on the section profile before anodization (Fig. 4(a)). When anodized for 5 min, oxide particles emerged in some region of the interface (Fig. 4(b)). Subsequently, the oxide particles grew up (Fig. 4(c)). At 20 min, the cross-section of the film was undulate and the thickness of the film was approximately 3 μm (Fig. 4(d)). At 30 min, the thickness of the film was comparatively thicker and smoother, being approximately 4μm. The thickness of the anodic oxide film was in relation to the ultimate value of anodizing forming voltage which was shown in Fig.1. The higher anodizing voltage was applied, the thicker anodic oxide films were formed.

3.3 Effect of anodization time on roughness of the anodic oxide films

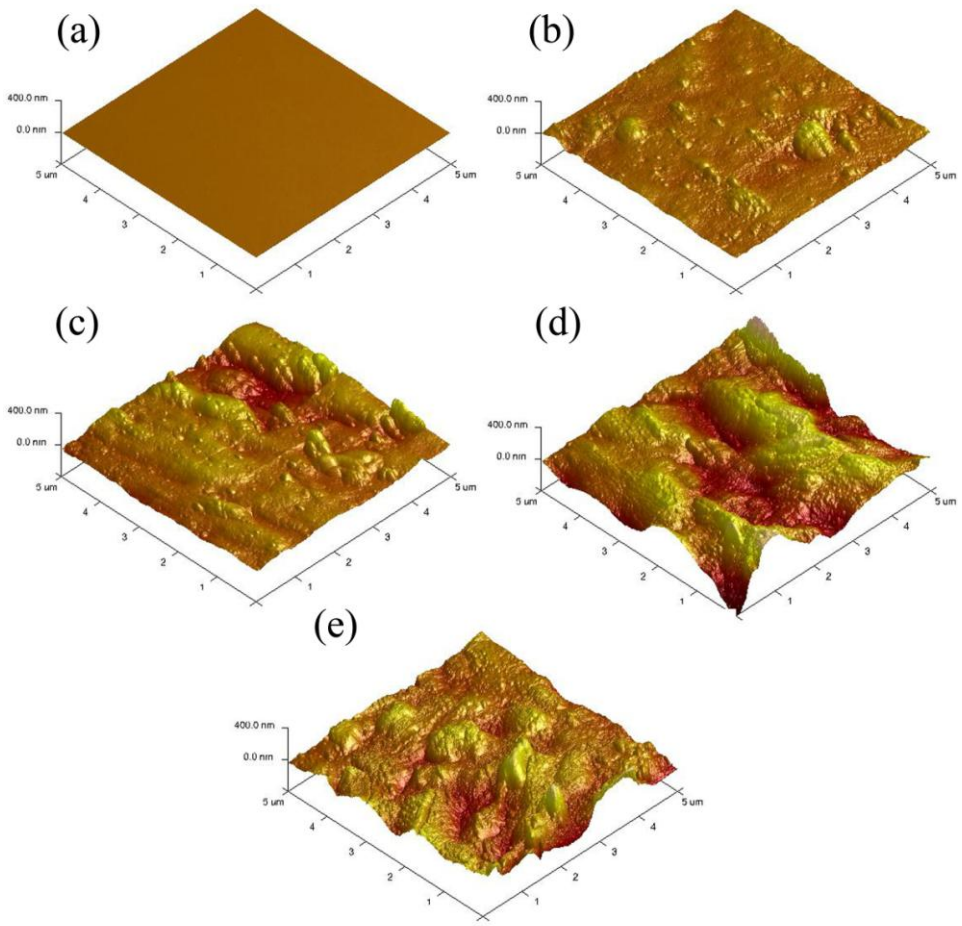

Figure 5. Three-dimensional AFM images of anodic oxide films on titanium alloy at different anodization time: (a) 0 min; (b) 5 min; (c) 10 min; (d) 20 min; (e) 30 min

Fig. 5 shows Three-dimensional AFM images of oxide films at different anodization time. The microscopy data was processed with NanoScope Analysis software and after completing the analysis, information regarding roughness was obtained. Fig. 6 shows the variation of root-mean-square roughness (Rq) and average roughness (Ra) derived from the AFM analysis of the recorded area (5 × 5 μm^2). In the initial stage of anodizing, the anodic oxide film is compact and the surface roughness is low. With longer anodization time, the surface roughness of oxide film increased before 20 min, which was due to the rupture of the compact inner layer in localized area and the nucleation of secondary oxide particles as seen in Fig. 5(c). The secondary oxide particle grew up and the number of secondary oxide particles increased with anodizing time as shown in Fig.5 (d, e). The appearance of non-uniformities in the oxide film caused an increase in surface roughness. However, the surface roughness decreased after 20 min. This was attributed to that a smooth secondary oxide layer which was composed of oxide particles had been formed.

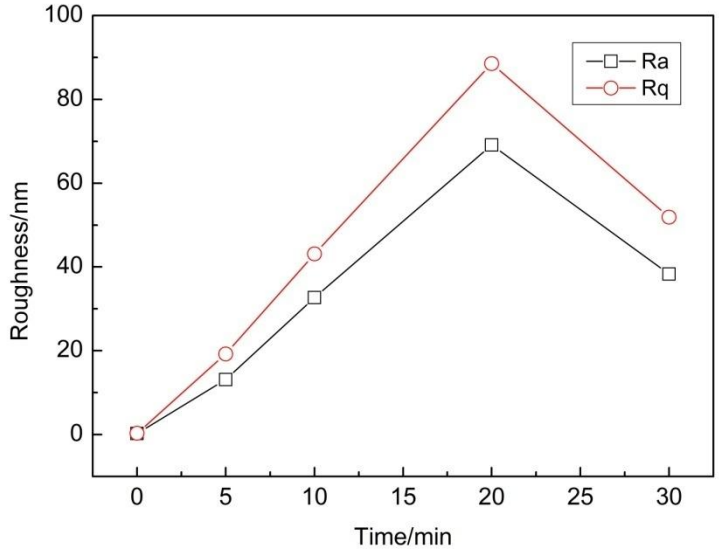

Figure 6. Surface roughness of anodic oxide films on titanium alloy at different anodization time

3.4 Effect of anodization time on crystal structure

Fig. 7 presented the Raman spectra of oxide films fabricated at different anodization time. The Raman peaks at 144, 196, 398, 520 and 639 cm^{-1} were characteristics of the anatase phase of TiO_2 [26]. The band at 144 cm^{-1} was very intense and sharp. It was assigned to vibrational mode with Eg symmetry. Another obvious intense band of the oxide films was at 610cm^{-1} and assigned to the B_{1g} vibrational mode. The peaks at 441 and 610 cm^{-1} which were due to rutile TiO_2[27]. Results showed that the films fabricated at different anodization time had the same crystal structure. The intensity of peaks increased with the increasing at anodization time. Hence, the longer the anodization time was and the more crystalline oxides (anatase and rutile) were. The intensity of the peaks corresponded to the amount of anodic oxide particles formed on the titanium alloy. The crystal structure of the anodic oxide films could be explained by the ultimate voltage. In general, at low voltages, the anodic oxide film was amorphous [19]. With increasing voltage, the structure of the oxide film changed from

amorphous to crystalline oxide. The voltage value increased with anodization time and the intensity of the peaks corresponded to the ultimate voltage value.

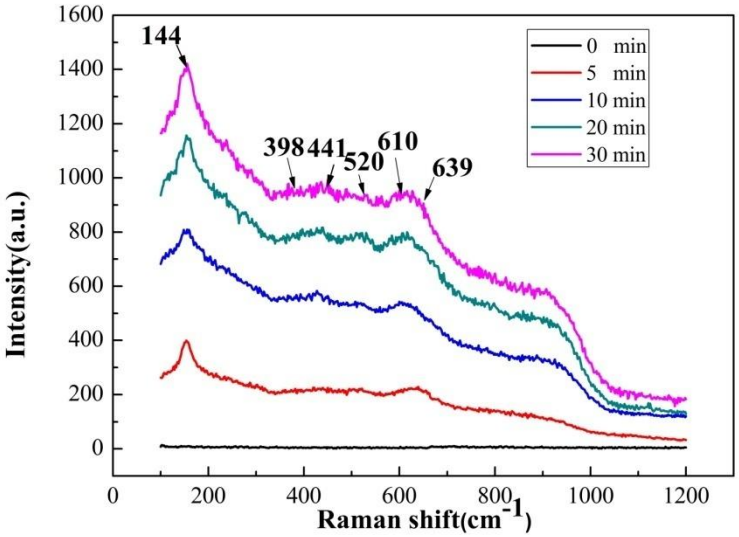

Figure 7. Raman spectra of anodic oxide films on titanium alloy at different anodization time

3.5 Effect of anodization time on EIS

Fig. 8 shows the EIS spectra of the anodic oxide films and the substrate in 0.2 M sodium tartrate solution. The | Z | bode plot shown in Fig. 8(a) reveals the impedance of anodized sample was higher than that of substrate. One time constant corresponding to the native passive film was observed for titanium alloy substrate in Fig. 8(b).

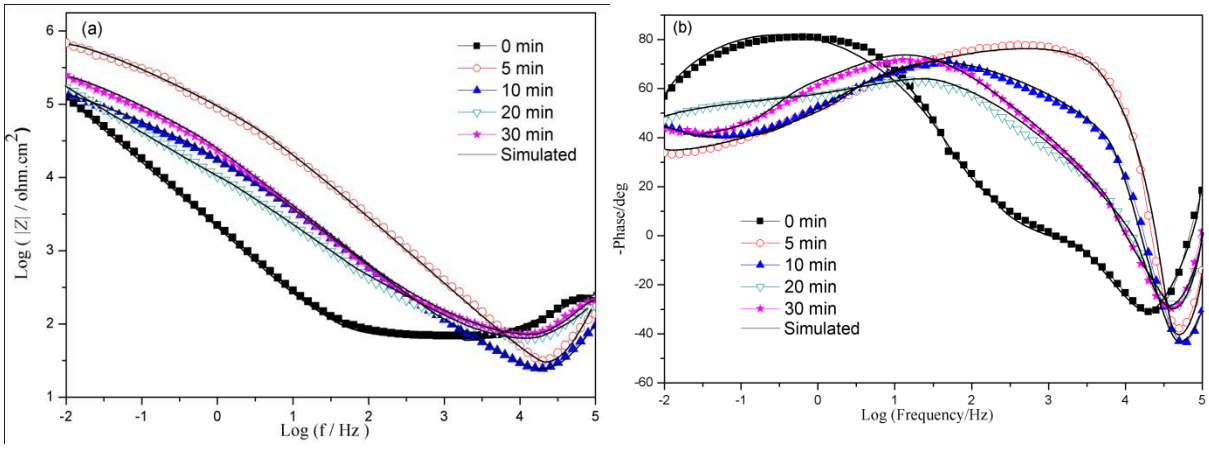

Figure 8. Bode plots of anodic oxide films on titanium alloy at different anodization time

Two time constants corresponding to a two-layer structure of the anodic oxide film were observed for anodized samples. The time constant appearing in high frequency corresponded to the

outer particle layer, whereas the time constant appearing in low frequency corresponded to the inner compact layer [28, 29].

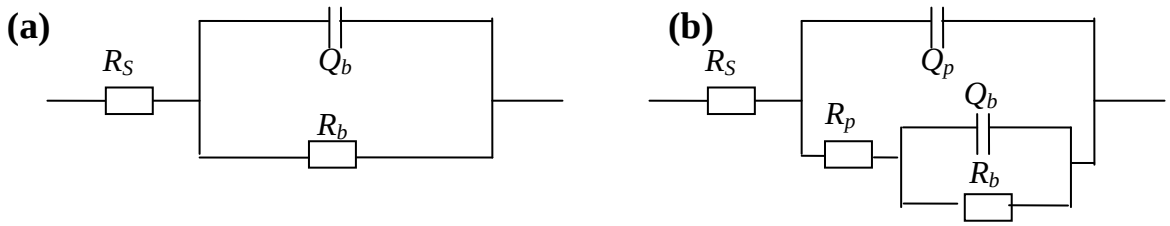

Figure 9. Equivalent circuit used for fitting electrochemical impedance data. (a) for substrate: R_S is the electrolyte resistance; R_b, Q_b are the resistance and capacitance of the native passive layer; (b) for anodized samples: R_b, Q_b are the resistance and capacitance of the inner layer; R_p, Q_p are the resistance and capacitance of the outer layer

As shown in Fig. 9(a), the EIS spectra were fitted and the model $R_S(Q_bR_b)$ was proposed. *Rs* was the electrolyte resistance. R_b was the resistance of native passive film and Q_b was the constant phase element (*CPE*) of passive film. Instead of capacitance *C* ,the *CPE* was used in the fitting because the former considers the fact that the barrier film never exhibited the theoretically expected phase shift of -90°and a slope of -1 for an ideal dielectric. In fact, the impedance of the constant-phase element (ZCPE) was defined by equation (1) as[30]:

$$Z_{CPE} = [Q(j\omega)^n]^{-1} \quad (1)$$

Where j was the imaginary unit and ω was the angular frequency ($\omega=2\Pi f$, with f being the frequency). In general, the *CPE* was given as both capacitance *Q* and factor *n*. The discussion about *Q* was complex because its physical meaning was still unclear. *n* was correlated with the fractal geometry of the material surface.

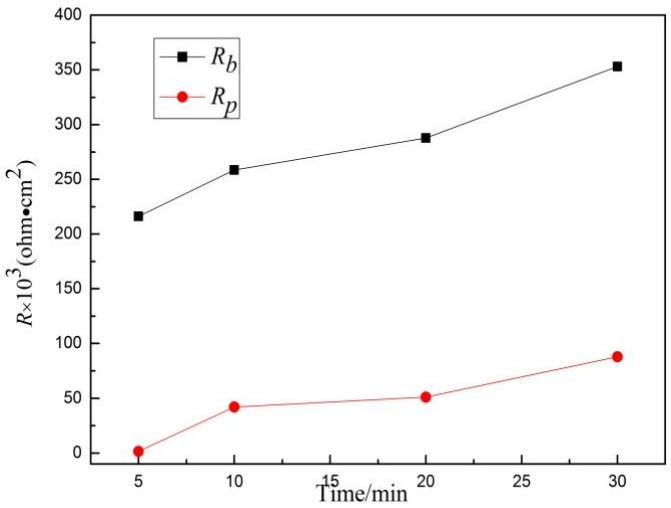

Figure 10. Variation of R_b and R_p of anodic oxide films formed at different anodization time

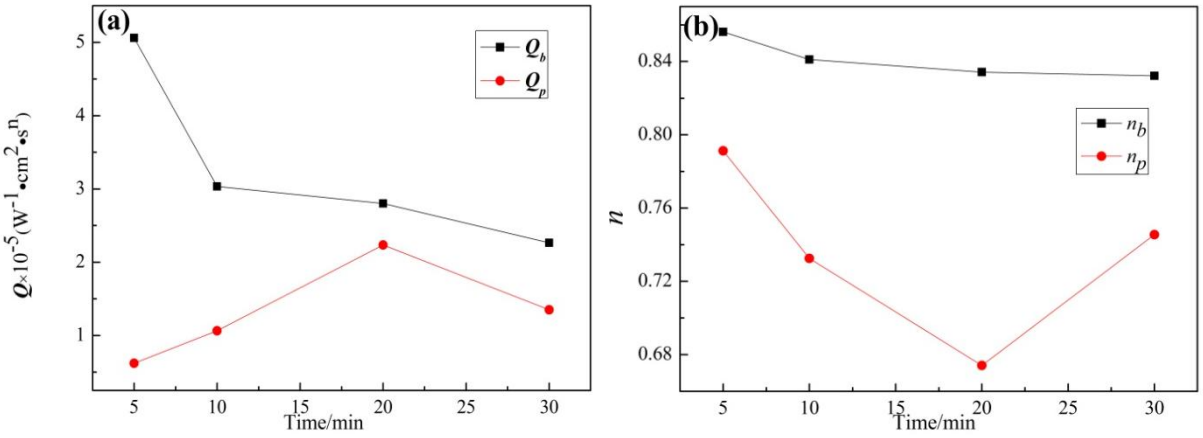

Figure 11. Variation of Q_p, Q_b (a) and n_p, n_b (b) of anodic oxide films formed at different anodization time

The equivalent circuit was shown in Fig. 9(b) and it was used to model the electrical response of the anodic oxide film, where *Rs* was the electrolyte resistance; Q_p and Q_b were the electrical properties of the outer and inner layer, respectively; R_p was the resistance of the outer layer; R_b represented the resistance of the inner layer. The quality of fitting to the equivalent circuit was judged by the chi-square value (below 1×10^{-3}) [28, 29].

The R_s represented the resistance of bulk electrolyte lying between the working and reference electrodes and the R_s value was very small. Fig. 10 showed variation of R_b and R_p of anodic oxide film formed at different anodization time. It could be seen that R_b is much higher than R_p, indicating that the resistance of the anodic oxide film strongly depended on the inner layer. The highest value of R_b was registered for the sample anodized 5 min, indicating the initial inner layer was quite compactness. The R_p value increased with anodizing time due to the increase in the film coverage and thickness, which was in agreement with the results of SEM and AFM analysis. At the early stage of anodization process, R_p value increased mainly due to the increase of coverage. In the later stage of anodization process, R_p value increased mainly due to increase in the film thickness.

As could be seen, Fig. 11 showed variation of Q_p, Q_b (a) and n_p, n_b (b)of anodic oxide film formed at different anodization time. In addition, according to Liu, the empirical exponent of the CPE was related to the fractal dimension, D_f, was correlated with the electrode/solution interfacial roughness[31], and its value increased with the roughness. *n* was inversely proportional to both D_f and the interfacial roughness[32]. The relation between *n* and D_f was shown in equation (2) as follows:

$$D_f = \frac{1}{n+1} \qquad (2)$$

As the anodization time increased, the value of n_p decreased before 20min, which indicated that the film anodized for 20 min had the highest roughness. The variation in the film roughness revealed by n_p could be confirmed by AFM results (Fig. 6). Q_b represented the electrical properties of the inner layer. The anodic oxide film had two interfaces: the film/electrolyte interface and the film/substrate interface. n_p reflected the inhomogeneity of the former interface, and therefore, n_b should reflect the inhomogeneity of the latter interface. A high value of n_b indicated that the film/substrate interface was

comparatively smooth. Little change of n_b over anodization time indicated that the substrate did not suffer serious corrosion by electrolyte during film growth.

4. CONCLUSIONS

1. Prolonging the anodization drastically changed the morphology and roughness of the anodic layer on titanium alloy substrates, fabricated in 0.2M $C_4H_4O_6Na_2$ using constant current mode. At the beginning of the anodization, a compact and uniform oxide layer was form on the substrates. With elongated anodization time, the inner layer ruptured locally and secondary oxide particles grew up. Finally, the secondary oxide particles aggregated in masses forming outer layer of anodic oxide films.

2. The surface roughness of oxide film increased before 20 min, which was due to localized rupture of the compact inner layer and nucleation of secondary oxide particles.

3. The uniformity of the surface and the relative intensity of anatase and rutile tended to increase with longer anodization time.

4. Detailed analysis of EIS results showed that the initial inner layer was quite compactness and the R_p value increased with anodizing time due to the increase in the coverage and thickness of the outer particle layer. The EIS results also showed that the substrate did not suffer serious corrosion by electrolyte during film growth.

ACKNOWLEDGEMENT
This work was supported by the National Natural Science Foundation of China (No. 51271012）and Fundamental Research Funds for the Central Universities.

References

1. Y. Liu, J.C.Zhu , Y.Wang, J.J.Zhan, *Materials Science and Engineering: A.*, 490(2008)113.
2. E.Vermessea,C. Mabrua,L.Arurault b , *Appl. Surf. Sci.,* 285(2013) 629.
3. A. Zhecheva, W. Sha, S. Malinov, *A. Surf. Coat. Technol*., 200 (2005), 2192.
4. C. Bayram, M.Demirbilek, E. Yalçın, M. Bozkurt, M. Doğan, E.B. Denkbaş, *Appl. Surf. Sci*., 288(2014) 143.
5. Y. Mizukoshi, N. Ohtsu, N. Masahashi, *Appl. Surf. Sci.,* 283(2013) 629.
6. S. Stojadinović, R. Vasilić, M. Petković, B. Kasalica, I. Belča, A. Žekić, Lj. Zeković, *Appl. Surf. Sci.*, 265(2013) 226.
7. N. Ohtsu, H. Kanno, S. Komiya, Y. Mizukoshi, N. Masahashi, *Appl. Surf. Sci*., 270(2013) 513.
8. H.J. Oh, C.S. Chi, *Mater. Lett.,* 86 (2012) 31.
9. Y.J. Park, K.H. Shin, H.J. Song, *Appl. Surf. Sci*., 253 (2007) 6013.
10. L. Xie, X. Liao, H. Xu, G. Yin, Z. Huang, Y. Yao, X. Chen, J. Gu, *Mater. Lett.,* 72 (2012)141.
11. H.Y. Si, Z.H. Sun, X. Kang, W.W. Zi, H.L. Zhang, *Micropor. Mesopor. Mater*.,119 (2009) 75.
12. D. Capek, M.-P. Gigandet, M. Masmoudi, M. Wery, O. Banakh, *Surf. Coat. Technol*.,202 (2008) 1379.
13. S. Komiya, K. Sakamoto, N. Ohtsu, *Appl. Surf. Sci*., 285(2014) 163.

14. N.Ohtsu, D.Ishikawa, S.Komiya, K.Sakamoto, *Thin Solid Films*., 556(2014) 247.
15. X.L.Zhang, Y.F.Zhang, L.M. Chang, Z.H Jiang, Z.P. Yao, X.W. Liu, *Materials Chemistry and Physics*., 132(2012) 909.
16. Z.P. Yao, Y.F. Liu, Y.J. Xu, Z.H. Jiang, F.P.Wang, *Materials Chemistry and Physics*., 126(2011)227.
17. J.H.Liu, J.L.Yi, S.M.Li, M. Yu, Y.Z.Yu. *Int. J .Miner Met Mater*., 16(2009) 96.
18. J.H.Liu, J.L.Yi, S.M.Li, M. Yu, G.L.Wu, L.Wu, *J. Appl. Electrochem*.,40(2010)1545.
19. J.H.Liu, G.L.Wu, M.Yu, L.Wu, Y.Zhang, S.M.Li, *Sur. Eng*.,28(2012)406.
20. S.M.Li, X.M.Yu, J.H.Liu, G.L.Wu, M.Yu, L.Wu,Y.Kang, *Int.J.Electrochem.Sci*.,8(2013)5438.
21. L.Young, *Trans. Faraday. Soc*., 50 (1954)159.
22. T. Okada, *J. Electrochem. Soc*., 132 (1985) 537.
23. Delplancke JL, Degrez M, Fontana A, Winand R, *Surf Coat Technol*., 16(1982)153.
24. H. Habazaki, M. Uozumi, H. Konno, K. Shimizu, P. Skeldon, G.E. Thompson, *Corrosion Sci*., 45 (2003) 2063.
25. X.F. Zhu, D.D. Li, Y. Song, Y.H. Xiao, *Mater. Lett*., 59 (2005) 3160.
26. X. Wang, J. Shen, Q. Pan, *J. Raman Spectrosc*., 42 (2011), 1578.
27. G. Chen, J.Chen, Z.K. Song, C. Srinivasakannan, J.H. Peng, *J. Alloys Comp*., 585 (2008), 75.
28. I. Milosev, T. Kosec, H.H. Strehblow, *Electrochim Acta*., 53 (2008) 3547.
29. S.A. Fadl-Allah, Q. Mohsen, *Appl. Surf .Sci.*, 256 (2010) 5849.
30. A.K. Shukla, R. Balasubramaniam, *Corros. Sci*., 48 (2006) 1696.
31. M. Keddam, H. Takenouti, *Electrochim. Acta*., 33 (1988) 445.
32. Z.P.Yao, Z.H.Jiang, S.G. Xin, X. T. Sun, X.H.Wu, *Electrochim Acta*., 50 (2005) 3273.